Medical Image Analysis 59 (2020) 101567

Contents lists available at ScienceDirect

Medical Image Analysis

journal homepage: www.elsevier.com/locate/media

Estimation of connectional brain templates using selective multi-view network normalization

Salma Dhifallah[a,b,*], Islem Rekik[a,c,*], for the Alzheimer's Disease Neuroimaging Initiative[1]

[a] BASIRA lab, Faculty of Computer and Informatics, Istanbul Technical University, Istanbul, Turkey
[b] National Engineering School of Sousse (ENISo), Sousse, Tunisia
[c] School of Science and Engineering, Computing, University of Dundee, United Kingdom

ARTICLE INFO

Article history:
Received 18 February 2019
Revised 23 September 2019
Accepted 27 September 2019
Available online 2 October 2019

Keywords:
Connectional brain template
Network normalization
Network analysis and fusion
Disordered connectional brain alterations

ABSTRACT

The brain connectome encodes different facets of the brain construct such as function and structure in a network. Noting that a brain network captures the individual signature of a particular subject, it remains a formidable challenge to extract a shared and representative brain signature across a population of brain networks, let alone *multi*-view brain networks. In this paper, we propose netNorm, a method that can meet this challenge by normalizing a population of multi-view brain networks, where each brain network represents a particular view of the brain, acquired using a neuroimaging technique. While conventional methods integrate the network views *equally* at a global scale, we propose a selective technique which unfolds the fusion process at a local scale by first selecting for each local pairwise connectivity between two anatomical regions of interest the *most representative cross-view feature vector* in the population. By combining the selected cross-view feature vectors, we then estimate a population representative tensor. Such multi-view representation captures the most shared traits across all subjects and thereby occupies a centered location compared to all views. In the final step, netNorm non-linearly fuses the frontal views of the estimated representative population tensor into a single network depicting the final brain connectional template. We demonstrate the broad applicability of our method on four connectomic datasets and we show that netNorm (i) produces the most centered and representative *connectional brain template* (CBT) that consistently captures the *unique* and *distinctive* traits of a population of multi-view brain networks, and (ii) identifies disordered brain connections by comparing templates estimated using disordered and healthy brains, respectively, demonstrating the *discriminative power* of the estimated CBTs. This allows to rapidly and efficiently spot atypical deviations from the normal brain connectome for comparative studies, circumventing the need to use machine learning techniques for discriminative feature identification.

1. Introduction

Neuroscientific and neuroimaging studies have relied heavily on the use of anatomical brain atlases for brain mapping, normalization and comparison across individuals and populations (Wu et al., 2015; Desikan et al., 2006; Dickie et al., 2017). However, the *connectional* aspect of the brain, captured by the wiring of its functional and structural neural connections, was overlooked with the exception of the work presented in (Rekik et al., 2017), which proposed the first work on estimating a brain network atlas using a population of unimodal brain networks using diffusive-shrinking graph technique. However, this work is only applicable to single-view brain networks, i.e. each brain is represented by a single network. Recently, Dhifallah et al. introduced in (Dhifallah and Rekik, 2019) the concept of population template for multi-view morphological networks using a cluster-based fusion technique. Despite its significant results, the performance of such method depends on the number of clusters used in the linear fusion step. Two of the main challenging obstacles for creating a connectional brain template for a population of multi-view brain networks lie essentially on the *inter-individual variability across subjects* for a

* Corresponding author.
E-mail addresses: salmadhifalah@gmail.com (S. Dhifallah), irekik@itu.edu.tr (I. Rekik).
URL: http://basira-lab.com (S. Dhifallah), https://github.com/basiralab/netNorm (I. Rekik)

[1] Data used in preparation of this article were obtained from the Alzheimer's Disease Neuroimaging Initiative (ADNI) database (adni.loni.usc.edu). As such, the investigators within the ADNI contributed to the design and implementation of ADNI and/or provided data but did not participate in analysis or writing of this report. A complete listing of ADNI investigators can be found at: http://adni.loni.usc.edu/wp-content/uploads/how_to_apply/ADNI_Acknowledgement_List.pdf.

https://doi.org/10.1016/j.media.2019.101567
1361-8415/

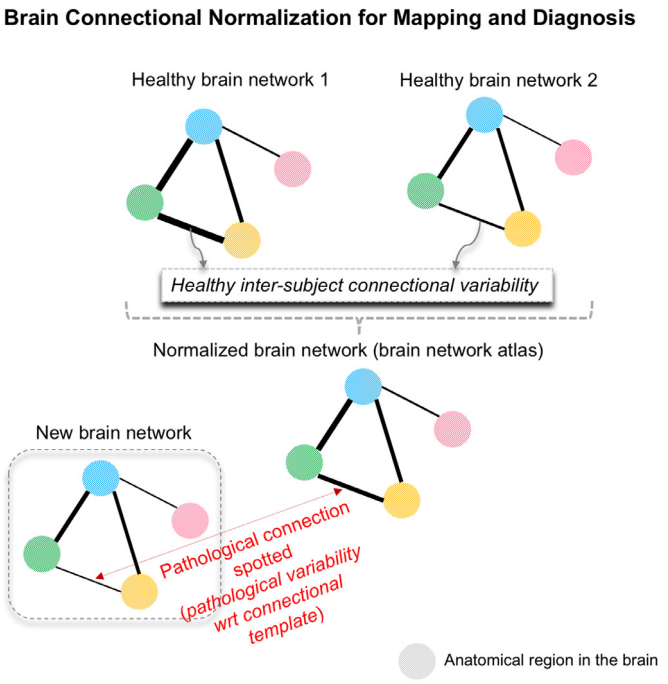

Fig. 1. Normalization of healthy brain networks for better spotting deviating pathological cases from the normalized connectional template.

given population, in addition to the multimodal aspect presented by the different views of the brain connectional construct. For instance, each view captures a particular aspect of the brain wiring offering different, yet, complementary information.

Recent technological advances in the field of medical imaging, in addition to the emerging international research initiatives, namely the ongoing 14 connectomic brain data gathering studies for Connectome Related to Human Disease (CRHD),[2] have given rise to large neuroimaging datasets (Essen et al., 2016) acquired using various magnetic resonance imaging (MRI) modalities (structural T1-weighted, diffusion, and functional MRI). The wealth of such multimodal and large datasets can provide an excellent tool for mapping human function and cognition (Holmes et al., 2015; Park et al., 2013; Seidlitz et al., 2018), in addition to enabling the discovery of novel population-based connectomic brain signatures for a deeper understanding of different connectional patterns of both the healthy and disordered brain (Hinrichs et al., 2011; Zhang et al., 2011; Yuan et al., 2012; Thung et al., 2014; Tong et al., 2015; Farrell et al., 2009). Yet, the diversity and complexity of such data now present a major data-analytic challenge to the field of neuroscience (Jbabdi et al., 2015). Namely, how can we integrate the complementary information offered by the different brain network views into a unified normalized connectional reference for comparative studies and classification? Moreover, how can we reduce inter-subject variability in both healthy and disordered populations for better identification of 'pathological' alterations in brain networks as deviations from the 'standard' brain network representation as described in Fig. 1?

In this paper, we propose netNorm, a novel framework that builds a connectional template for a population of multi-view brain networks. The key idea is to first create a representative tensor which is a mosaic representation capturing the most common cross-view feature vectors across subjects in a *selective manner*, then we *non-linearly* fuse the different layers of the representative tensor into the final unified connectional brain template (CBT). We refer to this network normalization method as netNorm (https://github.com/basiraLab/netNorm[3]). We demonstrate that netNorm outputs multi-view population-driven CBTs satisfying the following criteria: (i) they are well-centered and representative i.e., occupy the minimum distance to all brain views and to all subjects in a given population, and (ii) they can effectively and easily reveal discriminative brain connections that distinguish between two populations (e.g., healthy and demented brain networks) by well capturing population-specific traits and assuring robustness against inter-individual variance (Wu et al., 2011). netNorm is a simple and innovative framework that estimates multi-view brain connectional templates, thereby providing an integral representation of multi-view brain connections across subjects in a given population. More importantly, we also investigate the discriminative power of the estimated template in distinguishing between healthy and disordered brains. In other words, can we leverage the estimated connectional templates to spot disordered brain regions for disentangling different brain conditions (e.g., healthy *versus* disordered)?

2. Proposed netNorm framework

In the mid-1990s, Erich Fromm, a social psychological, introduced "the social character theory" on defining a society's psychological traits (Rickert, 1986). Unlike individual psychoanalysis, Fromm assumes that, at a group scale, psychological traits are no longer defined by the complete image of individual's psyche, rather it is based on the common psychological features across the group members. By analogy to Fromm's theory, if we consider that cross-view feature vectors capturing connectivity weights between pairs of ROIs across all views represent our population's traits, then a population template can be defined using the most common feature vectors across all subjects. Hence, we define a *commonality criterion* for each pair of ROIs using inter-subject feature vector distances. This criterion guides our cross-view feature vectors' selection process to construct a population representative brain tensor depicting the most common traits of our population across all subjects. Ultimately, by applying non-linear fusion, we then integrate the different views of the constructed tensor into a single connectivity network presenting the final population template.

In this section, we denote tensors by boldface Euler script letters, e.g., $\boldsymbol{\mathcal{X}}$. Matrices are denoted by boldface capital letters, e.g., $\boldsymbol{X}$, vectors are denoted by boldface lowercase letters, e.g., $\boldsymbol{x}$, and scalars are denoted by lowercase letters, e.g., x. For easy reference, we have summarized the major mathematical notations presented in this paper in Table 1.

We illustrate in Fig. 2 netNorm steps for brain connectional template estimation from multi-view connectomic data. First, for each subject in a population of interest, we build a population of multi-view brain networks by defining different morphological brain views. Then, for each pair of ROIs i and j, we define a cross-view feature vector combining their connectivity weights across all views. In the next step, we construct a high-order graph for each pair of ROIs i and j, modeling the relationship between the different subjects' feature vectors. Using the defined graph, we then define a commonality criterion guiding a feature vector selection process. We repeat the same process for all cross-view feature vectors created for each pair of ROIs in order to construct the population representative tensor. The final CBT is then obtained by applying non-linear fusion for different representative tensor views.

2.1. Multi-view morphological brain network construction

The two most widely used measures of brain connectivity for mapping brain wiring in the literature are functional connectivity

[2] https://www.humanconnectome.org/disease-studies.

[3] The code will be released upon the acceptance of the paper.

Table 1
Major mathematical notations used in this paper.

Mathematical notation	Definition
N	Total number of subjects in the population
n_v	Total number of brain views for each subject
n_r	Total number of regions of interest in the brain
$\mathcal{T}^s$	Subject's representative tensor $\in \mathbb{R}^{n_r \times n_r \times n_v}$
$\boldsymbol{X}_k^s$	k^{th} network view for subject $s \in \mathbb{R}^{n_r \times n_r}$
$\boldsymbol{V}_{ij}^s$	Feature vector for subject s related to ROIs i and $j \in \mathbb{R}^{n_v \times 1}$
$\boldsymbol{H}_{ij}$	High-order graph (graph of a graph) for pair of ROIs i and $j \in \mathbb{R}^{N \times N}$
$\tilde{\mathcal{T}}$	Population's representative tensor $\in \mathbb{R}^{n_r \times n_r \times n_v}$
$\tilde{\boldsymbol{X}}_v$	v^{th} population's representative brain view $\in \mathbb{R}^{n_r \times n_r}$
$\boldsymbol{P}_v$	Status matrix for view $v \in \mathbb{R}^{n_r \times n_r}$
$\boldsymbol{S}_v$	Kernel matrix for view $v \in \mathbb{R}^{n_r \times n_r}$
$\mathbf{A}$	Estimated connectional brain template (or atlas) $\in \mathbb{R}^{n_r \times n_r}$

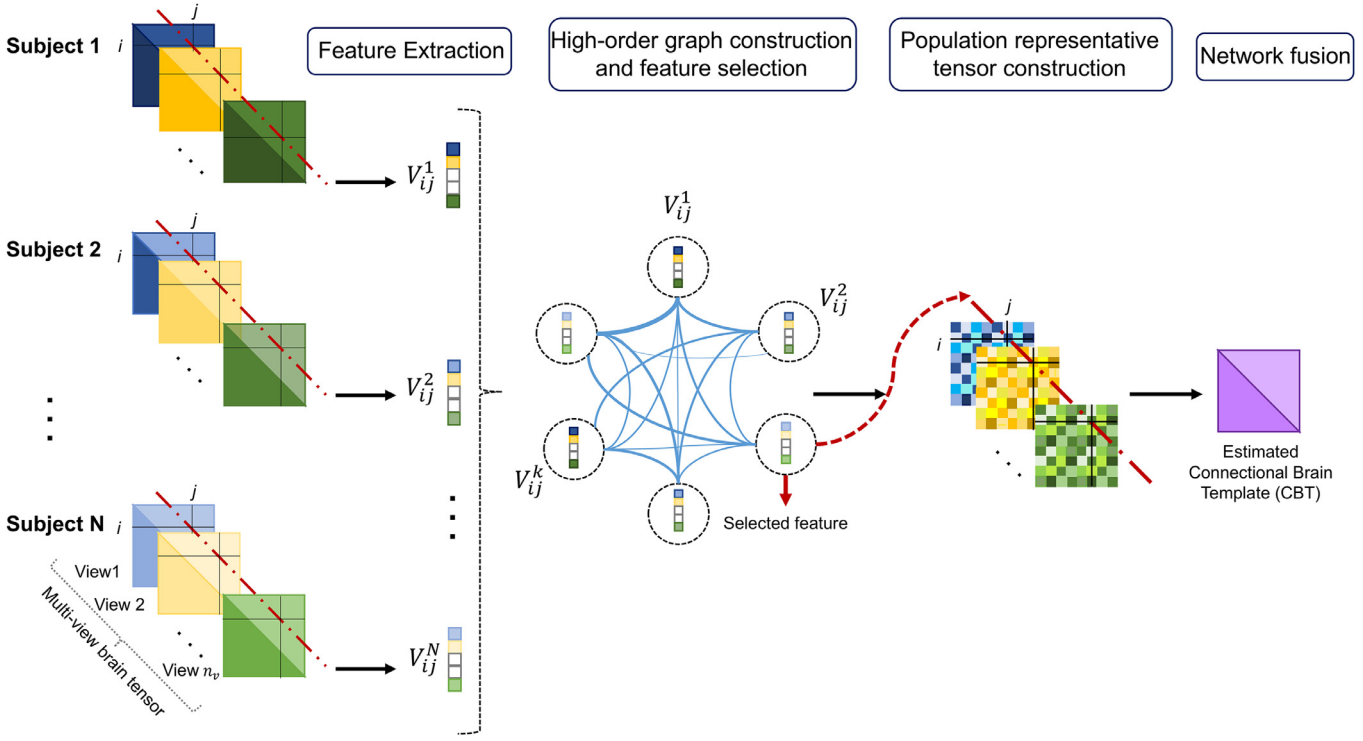

Fig. 2. Overview of netNorm pipeline for connectional brain template (CBT) estimation from multi-view brain networks. Given a population of N multi-view tensors, where each subject-specific tensor comprises a set of stacked brain network views, we first extract a feature vector $\boldsymbol{V}_{ij}^k$ for each subject k and each pair of brain regions of interest (ROIs) i and j. Each feature vector $\boldsymbol{V}_{ij}^k$ is composed of connectivity weights between ROIs i and j derived from all views. Next, for each pair of ROIs, we construct a high-order graph modeling inter-subject relationship. Each graph node embeds a feature vector $\boldsymbol{V}_{ij}^k$ for subject k in the population and the strength of an edge connecting two nodes k and k is calculated as the Euclidian distance between $\boldsymbol{V}_{ij}^k$ and $\boldsymbol{V}_{ij}^{k'}$. The node satisfying the minimum mean distance to all other nodes is then selected as a population-specific feature vector representative. By selecting the optimal population-specific feature vectors for each pair of ROIs, we construct the population representative tensor $\tilde{\mathrm{T}}$. Finally, we generate brain connectional template by non-linearly fusing all tensor layers using similarity network fusion (SNF) technique.

and structural connectivity, derived from functional magnetic resonance imaging (fMRI) and diffusion weighted imaging (DWI), respectively (Lerch et al., 2017). Yet, these imaging techniques present the limitations of time-consumption, high cost and proneness to noise (Lisowska et al., 2018). Recent works (Lisowska et al., 2018; Mahjoub et al., 2018; Raeper et al., 2018; Soussia et al., 2018) have considered the use of morphological connectional features in order to circumvent these limitations. Brain morphology including cortical measures (e.g., cortical thickness) can be used as biomarkers for neurodevelopmental (i.e., ASD) (Wallace et al., 2010; Hardan et al., 2009) and neurodegenerative (i.e., AD) diseases (McEvoy et al., 2009; Ridgway et al., 2012). More specifically, brain morphological changes may reflect abnormal functional and structural connections (Essen, 1997). Inspired by these works (Lisowska et al., 2018; Mahjoub et al., 2018; Raeper et al., 2018; Soussia et al., 2018) as well as the work of (Seidlitz et al., 2018) investigating the relation between morphological similarity networks and cognition, we propose to evaluate netNorm using multi-view brain morphological networks derived from different morphological measurements relating brain regions to one another. Hence, for each subject in the population, we define a single-view morphological brain network (MBN) as a graph where nodes represent cortical regions of interest (ROIs) and edges encode the interconnections between different nodes capturing their dissimilarity in morphology using a specific cortical attribute (e.g., cortical thickness, sulcal depth). More specifically, we represent each network as a matrix $\boldsymbol{X}$ in $\mathbb{R}^{n_r \times n_r}$, where n_r represents the number of ROIs. For each ROI, we first compute the average value of a cortical attribute. Next, we define each element $\boldsymbol{X}(i, j)$ as the absolute difference between the average cortical attributes in ROIs i and j, denoting the weight of the link between both regions of interest. Using different morphological measurements, we can

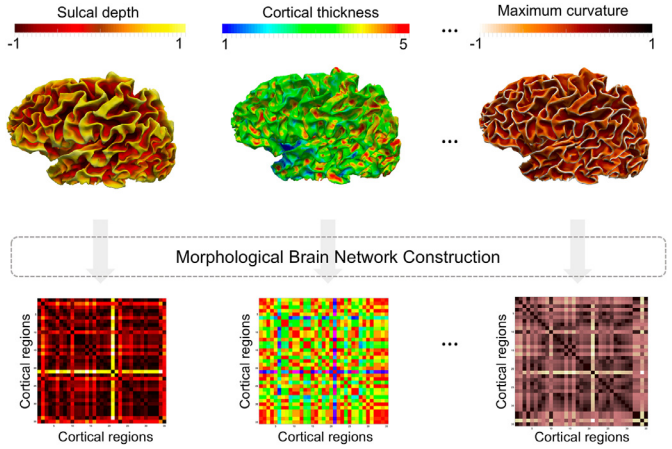

Fig. 3. Morphological brain network construction for a representative subject using different views of the cortical surface. Each view is represented by a matrix quantifying the dissimilarity between each pair of ROIs in the brain in terms of a specific morphological attribute (e.g., sulcal depth, cortical thickness).

generate multiple network views for each individual, where each view is represented by an $n_r \times n_r$ connectivity matrix (Fig. 3). Given a population of N subjects where each subject s is represented by n_v brain network views, let $\boldsymbol{X}_k^s$ denote the k^{th} network view (or matrix) for subject s. We can then represent each subject s by a tensor $\mathrm{T}^s \in \mathbb{R}^{n_r \times n_r \times n_v}$ where its k^{th} frontal view represents a brain connectivity matrix $\boldsymbol{X}_k^s$. Note that we set the diagonal for each matrix $\boldsymbol{X}_k^s$ to zero in order to avoid self-similarity.

2.2. Connectional feature extraction

For each subject s, we define a cross-view feature vector (weight vector) $\boldsymbol{V}_{ij}^s$; $1 \le i, j \le n_r$ for each pair of ROIs i and j. Specifically, $\boldsymbol{V}_{ij}^s$ captures the connectivity between ROIs i and j across all views. Each subject-specific feature vector is defined as follows:

$$\boldsymbol{V}_{ij}^s(k) = \mathcal{T}^s(i, j, k), \forall\ 1 \le k \le n_v,\ \ \forall\ 1 \le i, j \le n_r$$

Considering that brain networks can be represented as symmetric matrices with null diagonal, we only use the upper triangular part, thereby decreasing the total number of cross-view feature vectors for each subject from n_r^2 to $N_f = \sum_{i=1}^{n_r-1}(n_r - 1) = \frac{n_r(n_r-1)}{2}$.

2.3. High-order graph construction

In order to unravel the complex relationships between subjects in a specific population for the normalization process, we propose to build an $N \times N$ high-order graph $\boldsymbol{H}_{ij}$ for each pair of ROIs i and j (i.e., for each brain connectional feature vector). Such a high-order representation would help reveal cross-view feature vectors' dissimilarities across subjects for a given population by computing the inter-individual distances for each pairwise feature vector. For a pair of ROIs i and j, $\boldsymbol{H}_{ij}$ is composed of a set of N nodes $\{\boldsymbol{V}_{ij}^1, \ldots, \boldsymbol{V}_{ij}^N\}$, each representing a subject-specific cross-view feature vector $\boldsymbol{V}_{ij}^s$ for a subject s. The edges are calculated based on the Euclidean distance between feature vectors for each pair of subjects in the population. For ROIs i and j, the edge between subjects s and s' is calculated as follows:

$$\boldsymbol{H}_{ij}(s, s') = \sqrt{\sum_{k=1}^{n_v} \left(\boldsymbol{V}_{ij}^s(k) - \boldsymbol{V}_{ij}^{s'}(k)\right)^2};\ \forall\ 1 \le s, s' \le N$$

2.4. Quantifying the centeredness of each subject for a specific pair of ROIs

For each pair of ROIs i and j, we construct an $N \times 1$ distance vector $\boldsymbol{D}_{ij}$ calculated by summing $\boldsymbol{H}_{ij}$ rows:

$$\boldsymbol{D}_{ij}(s) = \sum_{s'=1}^{N} \boldsymbol{H}_{ij}(s, s') = \sum_{s'=1}^{N} \sqrt{\sum_{k=1}^{n_v} \left(\boldsymbol{V}_{ij}^s(k) - \boldsymbol{V}_{ij}^{s'}(k)\right)^2}$$

Where $\boldsymbol{D}_{ij}^{(s)}$ is the cumulative distance from a feature vector $\boldsymbol{V}_{ij}^s$ for subject s to all remaining subjects in the population, $\boldsymbol{V}_{ij}^{s'}$, $\forall\ 1 \le s' \ne s \le N$. The intuition behind this step is to define an inclusiveness (commonality) criterion for each feature type across the whole population, where the feature vector satisfying the smallest distance $\min_{1 \le s \le N} \boldsymbol{D}_{ij}(s)$ depicts the most representative and centered trait (cross-view feature vector) across all subjects.

2.5. Population-representative tensor construction

Instead of using the whole population dataset to build the final CBT, netNorm constructs a population-representative tensor $\tilde{\mathcal{T}}$ as follows:

$$\tilde{\mathcal{T}}(i, j, k) = \boldsymbol{V}_{ij}^{s'}(k);\ \ \forall\ 1 \le k \le n_v;\ \ where\ s' = \min_{1 \le s \le N} \boldsymbol{D}_{ij}(s)$$

In essence, $\tilde{\mathcal{T}}$ is constructed using a selection process that takes into consideration 'the best' cross-view feature vectors (nearest feature to all others). The intuition behind this step is to define a multimodal brain network that captures the most shared traits of the population while 'overlooking' the peculiarities of individual subjects which is the case for network brain average that treats all subjects equally in the fusion process.

2.6. Non-linear fusion for connectional brain template estimation

Since the relationship between brain connections across views is complex and nonlinear, netNorm non-linearly merges the n_v views of the population's representative tensor $\tilde{\mathcal{T}}$ in order to obtain the final CBT. To this aim, we use similarity network fusion (SNF) introduced by Wang et al. in(Wang et al., 2014). SNF is a framework that integrates networks defined using different data types for a same set of samples into a single network that gathers both local and global traits of similarities between samples. This final matrix is then used for retrieval, clustering or classification.

In our case, we leverage SNF technique to generate a CBT using the n_v network views composing $\tilde{\mathcal{T}}$. The first step is to initially construct a status matrix $\boldsymbol{P}_v$ for each view v carrying the whole information about ROIs' connections and a local matrix $\boldsymbol{S}_v$ that only takes into consideration the connections to the K nearest neighbours of each ROI. This fusion technique is based on iteratively updating each individual status network $\boldsymbol{P}_v$ in the population through diffusing the average global structure of other $N-1$ networks along the individual local sparse matrix $\boldsymbol{S}_v$. $\boldsymbol{P}_v$ and $\boldsymbol{S}_v$ are calculated as follows:

$$\boldsymbol{P}_v(i, j) = \begin{cases} \frac{\tilde{\boldsymbol{X}}_v(i,j)}{2\sum_{l \ne i} \tilde{\boldsymbol{X}}_v(i,l)}, & j \ne i \\ 1/2, & if\ i = j \end{cases}$$

$$\boldsymbol{S}_v(i, j) = \begin{cases} \frac{\tilde{\boldsymbol{X}}_v(i,j)}{\sum_{l \in N_i} \tilde{\boldsymbol{X}}_v(i,l)}, & j \in N_i \\ 0 & \text{otherwise} \end{cases}$$

Where $\tilde{\boldsymbol{X}}_v$ is the v^{th} frontal view of $\tilde{\mathcal{T}}$ denoting the v^{th} population's representative brain view, and N_i is the set of neighbors of

Algorithm 1 SNF algorithm for fusing matrices (Wang et al., 2014).

1: Inputs:
A set of m similarity matrices: $\boldsymbol{W_k}(i, j)$
2: Defining a status matrix for each similarity matrix $\boldsymbol{W_k}$:
for each matrix $\boldsymbol{W_k}$ **do**
  for each pair of ROIs i and j **do**

$$\boldsymbol{P_k^0}(\boldsymbol{i}, \boldsymbol{j}) = \begin{cases} \frac{\boldsymbol{W_k}(\boldsymbol{i},\boldsymbol{j})}{2\sum_{l\neq i}\boldsymbol{W_k}(\boldsymbol{i},\boldsymbol{l})}, & j \neq i \\ 1/2, & j = i \end{cases}$$

  end
end
3: Defining the K nearest neighbours for each ROI $\boldsymbol{x_i}$ and for each view $\boldsymbol{k}$:
for each matrix $\boldsymbol{W_k}$ **do**
  for each ROI i **do**
  Find the K nearest neighbours N_i for each ROI x_i:
  N_i corresponds to the K ROIS x_l where $\boldsymbol{W_k}(\boldsymbol{i}, \boldsymbol{l})$ is maximum.
  end
end
4: Defining a local matrix for each similarity matrix $\boldsymbol{W_k}$:
for each matrix $\boldsymbol{W_k}$ **do**
  for each pair of ROIs i and j **do**

$$\mathbf{S_k}(\boldsymbol{i}, \boldsymbol{j}) = \begin{cases} \frac{\boldsymbol{W_k}(\boldsymbol{i},\boldsymbol{j})}{\sum_{k\in N_i}\boldsymbol{W_k}(\boldsymbol{i},\boldsymbol{l})}, & j\in \boldsymbol{N_i} \\ 0, & \boldsymbol{otherwise} \end{cases}$$

  end
end
5: Iteratively updating the status matrix for each view $\boldsymbol{k}$:
for each view k do

$$\boldsymbol{P_k^{t+1}} = \mathbf{S_k}\left(\frac{\sum_{v\neq k}\boldsymbol{P_v^t}}{\boldsymbol{m}-1}\right)(\mathbf{S_k})^T,\ k = 1 \ldots m$$

end
6: Defining the final fused similarity matrix:

$$\boldsymbol{P_c} = \frac{\sum_{1\leq k\leq m}\boldsymbol{P_k^t}}{\boldsymbol{m}}$$

ROI i. This is achieved through iteratively updating the following equation:

$$\boldsymbol{P_v^t} = \boldsymbol{S_v} \times \left(\frac{\sum_{v'\neq v}\boldsymbol{P_{v'}^t}}{n_v - 1}\right) \times (\boldsymbol{S_v})^T$$

Where $t \in \{0, \ldots, t^*\}$ denotes the diffusion iteration number and T denotes the matrix transpose operator. Finally, following t^* iterations, the target CBT is generated by averaging all updated diffused networks:

$$\boldsymbol{A} = \frac{1}{n_v}\sum_{k=1}^{n_v}\boldsymbol{P_v^{t^*}}$$

Remark on using SNF to fuse dissimilarity matrices. Originally, SNF technique (Wang et al., 2014) is used to fuse similarity networks for clustering purposes. In this remark, we mathematically demonstrate that SNF can be also applied to fuse dissimilarity data where the different connections between ROIs denote distance measures. We introduce below the different steps of SNF algorithm for data fusion as introduced in (Wang et al., 2014).

Considering Algorithm 1, we note that while the different steps (1, 2, 5 and 6) are mathematically applicable to any type of data (dis/similarity), step 3 and 4 consider pairwise similarities within a network and use them as a reference for uncovering the inner structure of the input data by defining the local matrix for each view. The question that arises at this point is: "*Is this technique applicable for dissimilarity networks where the connectivity values denote distances instead of similarities?*"

The essential role of defining the local matrix $\boldsymbol{S_k}$ for a view k is to unravel the local structure of the sample matrices in terms of strong and weak connections. For similarity matrices, we aim to enhance similarities across ROIs, while for dissimilarity matrices, we aim to discover the strongest connections in terms of distance measures (dissimilarities).

According to SNF algorithm (Algorithm 1, Wang et al., 2014), the set of most similar ROIs $N_i = \{x_j\}_j$ to each ROI x_i are defined by choosing the first K regions x_j with the maximum connectivity measure $\boldsymbol{W}_k(i, j)$. The intuition behind this step is to define a local matrix $\boldsymbol{S}_k$ capturing the local structure of the network. Only strong connections denoting the most similar connections remain strong while weak connections disappear. Integrating $\boldsymbol{S}_k$ into the fusion process would help enhance the strong similarity connections across networks. In case where the input networks are encoded in dissimilarity matrices as in our experiments, the connections between pairs of ROIs denote the distance between them. Hence, larger values represent most dissimilar pairs of ROIs. Applying step 3 in Algorithm 1, by picking the top ROIs with the maximum connectivity values to an ROI x_i, we are enhancing the dissimilarity between pairs of ROIs across all views. The local structure of the networks would then denote the local dissimilarities across ROIs while reducing the most similar connections. Using the local matrix $\boldsymbol{S}_k$ in the fusion process, strong dissimilarities will get stronger and weak dissimilarities will get weaker. For better reference, we present in Fig. 4 an example illustrating the definition of local matrices for both similarity and dissimilarity sub-networks.

In conclusion, from a mathematical perspective, the different steps of SNF algorithm are applicable to both similarity and dissimilarity networks. Therefore, SNF can be used to fuse any type of data regardless of the nature of their inner connection. □

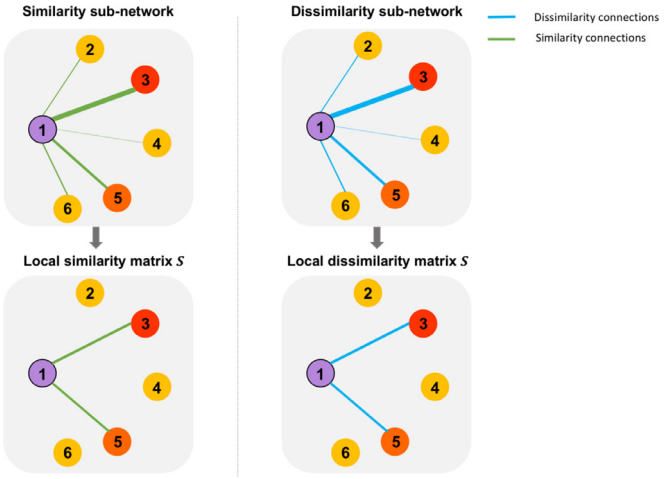

Fig. 4. Illustration of SNF local matrix derived from similarity and dissimilarity sub-networks centered at a single seed node (purple node). Strong connections in terms of similarity and dissimilarity measures are respectively transformed into similarity and dissimilarity local matrices after normalization where weak connections disappear for both. The number of neighbors K is set to 2 and the neighborhood for node 1 is defined as $N_1 = \{x_3, x_5\}$ in both sub-networks.

Table 2
Data distribution for LMCI/AD and NC/ASD datasets.

Datasets	AD/LMCI		ASD/NC	
	AD	LMCI	ASD	NC
Number of subjects	41	36	155	186
Male	23	20	140	155
Female	18	16	15	31
Mean age	75.27	72.54	16.92	16.65

3. Experiments and material

3.1. Evaluation connectomic datasets

We evaluated netNorm on two datasets as detailed in Table 2, where each subject is represented by four morphological brain networks. The first dataset (ASD/NC dataset) is collected from

the Autism Brain Imaging Data Exchange ABIDE I public dataset[4] and consists of 341 subjects: 155 normal controls (NC) and 186 subjects with autism spectrum disorder (ASD) (Martino et al., 2014). The second dataset (LMCI/AD dataset) is collected from Alzheimer's Disease Neuroimaging Initiative (ADNI) database GO public dataset[5] consisting of 77 subjects: 36 subjects with Late Mild Cognitive Impairment (LMCI) and 41 subjects with Alzheimer disease (AD) (Mueller et al., 2005). The ADNI was launched in 2003 as a public-private partnership, led by Principal Investigator Michael W. Weiner, MD. The primary goal of ADNI has been to test whether serial magnetic resonance imaging (MRI), positron emission tomography (PET), other biological markers, and clinical and neuropsychological assessment can be combined to measure the progression of mild cognitive impairment (MCI) and early Alzheimer's disease (AD).

We used FreeSurfer pipeline (Fischl, 2012) to reconstruct both right and left cortical hemispheres (RH and LH) for each subject from structural T1-weighted MRI. We parcellated each hemisphere into 35 cortical regions of interest using Desikan-Killiany atlas (Fischl et al., 2004). Finally, we generated 4 cortical morphological brain views (networks) for each hemisphere as shown in Fig. 3: $\boldsymbol{X}_1$, $\boldsymbol{X}_2$, $\boldsymbol{X}_3$ and $\boldsymbol{X}_4$ denoting respectively the maximum principal curvature, the mean cortical thickness, the mean sulcal depth, and the average curvature.

Source code. netNorm source code is available at https://github.com/basiralab/netNorm.

3.2. Evaluation of connectional brain template representativeness

To evaluate the centeredness and representativeness of the estimated CBT in the original manifold where all multi-view networks are nested, we calculate the mean Frobenius distance from each view of each subject in the population to the estimated template. The mean Frobenius distance between 2 matrices **A** and **B** is calculated as: $d_F(A, B) = \sqrt{\sum_i \sum_j |a_{ij} - b_{ij}|^2}$. For reproducibility and generalizability, we used 5-fold cross-validation where we divided each population into 5 sub-populations. We used each sub-population to generate a connectional template and calculate its distance to all views within the subgroup. Hence, for each population (e.g., ASD), we generated 5 CBTs, with an additional one using the whole data.

For a clear representation of the results, we normalize the Frobenius distances calculated using netNorm and state-of-the-art techniques within each fold using the following formula:

$$d'_F = (d_F - mean_i)/(max_i - mean_i) + 1.5$$

Where $mean_i$ and max_i denote respectively the average and the maximum values of the Frobenius distances calculated using the different distances for a given fold i.

To assess the statistical significance of netNorm, we validated the comparative study of the CBTs centredness using a two-tailed paired t-test across all data folds in addition to the whole data between netNorm and each of the comparative methods.

3.3. Evaluation of connectional brain template discriminability

In order to test the discriminability of the estimated CBTs, we conducted a group comparison study to identify the top brain ROIs that distinguish between two groups: (1) ASD vs. NC, and (2) LMCI vs. AD, respectively, using both left and right hemispheres. For this aim, we estimated a MV-CBT for each group, then by computing the difference between both templates (e.g., NC and ASD templates) we identified the top 15 ROIs that distinguish between both groups. Next, we computed the overlap (in%) between the top discriminative ROIs found by netNorm and a supervised machine learning method based on multiple kernel learning (MKL). Both methods are detailed bellow.

3.3.1. Top discriminative ROIs identification using the estimated CBTs

To assess the reproducibility of CBT produced by netNorm, we used randomized 5-fold partition to divide each population p and p' into 5 folds: p_i and p'_j, respectively, where $1 \leq i, j \leq 5$. $\boldsymbol{A}_i^p$ and $\boldsymbol{A}_j^{p'}$ denote the estimated CBT for the i^{th} fold in p and the j^{th} fold in p'. We compute the mean absolute difference between the estimated templates across folds using a simple inter-template subtraction as follows:

$$\boldsymbol{D} = \sum_{i,j=1}^{5} \left| \boldsymbol{A}_i^p - \boldsymbol{A}_j^{p'} \right|$$

Where $\boldsymbol{D}$ is an $n_r \times n_r$ matrix containing absolute features' differences between fold p_i and fold p'_j in terms of connectional strength. By summing the columns of $\boldsymbol{D}$, we obtain a score vector $\boldsymbol{\alpha}$ where the i^{th} coefficient denotes the score α_i assigned to the i^{th} ROI representing the cumulative distance from ROI i to all other ROIs $k \neq i$. α_i is calculated as follows:

$$\alpha_i = \sum_{\substack{k=1 \\ k \neq i}}^{n_r} \boldsymbol{D}(i,k)$$

The top discriminative ROIs are then identified as those with the highest scores (Fig. 5).

3.3.2. Top discriminative ROIs identification using MKL

Multiple kernel learning (MKL) is a technique aiming to identify the most discriminative features for a target classification task that distinguishes between two classes p and p'. Given a set of labelled data, each represented by a feature vector, we train a support vector machine (SVM) classifier that learns a weight for each feature type quantifying its discriminative power in the classification task.

For each network view, we used 5-fold randomized partitioning of data samples to divide each population p and p' into 5 subpopulations. Given the v^{th} brain view, for each combination of subpopulations p_i and p'_j, where $1 \leq i, j \leq 5$, a connectional feature vector $\boldsymbol{F}_s^v$ is constructed for each subject s in both subpopulations using the vectorized upper triangular part of the connectivity matrix $\boldsymbol{X}_s^v$. We assign a label $y_s^v \in \{\pm 1\}$ for each feature vector $\boldsymbol{F}_s^v$ denoting the population class. Feature vectors and their labels are then used as inputs to train an SVM classifier. Using wrapper method, a weight vector $\boldsymbol{w}_{ij}^v$ is estimated to assign a weight score for each feature (connectional strength) in the classification process using view v and subpopulations p_i and p'_j. The final weight vector $\boldsymbol{w}$ is then calculated by summing up the weight vectors across all views and all combinations of subpopulations:

$$\boldsymbol{w} = \sum_{v=1}^{n_v} \sum_{i,j=1}^{5} \boldsymbol{w}_{ij}^v$$

Then, we assign a score value α_i to the i^{th} ROI by adding up the weights of all connections involving ROI i to other ROIs. Let $\boldsymbol{w}(i, j)$ denote the weight of the connectivity strength between ROIs i and j, α_i is then calculated as follows:

$$\alpha_i = \sum_{j \neq i} \boldsymbol{w}(i,j)$$

[4] http://fcon_1000.projects.nitrc.org/indi/abide/.

[5] Data used in preparation of this article were obtained from the Alzheimer's Disease Neuroimaging Initiative (ADNI) database (adni.loni.usc.edu). As such, the investigators within the ADNI contributed to the design and implementation of ADNI and/or provided data but did not participate in analysis or writing of this report. A complete listing of ADNI investigators can be found at: https://adni.loni.usc.edu/wp-content/uploads/how_to_apply/ADNI_Acknowledgement_List.pdf.

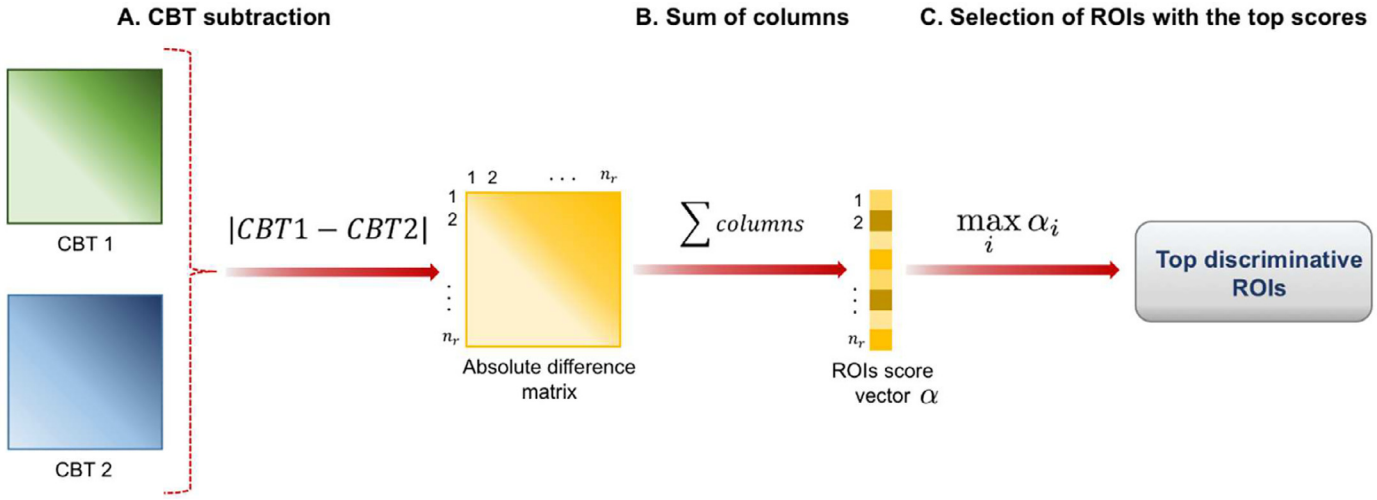

Fig. 5. Identification of the top 15 discriminative regions of interest (ROIs) using the estimated connectional brain templates (CBTs) by netNorm. (A) We compute the absolute element-wise difference between both CBTs to generate the absolute difference matrix. (B) By summing up the column elements of each row in the absolute difference matrix, we create a score vector assigning the weight for each ROI. (C) Top discriminative ROIs are then identified using the highest scores.

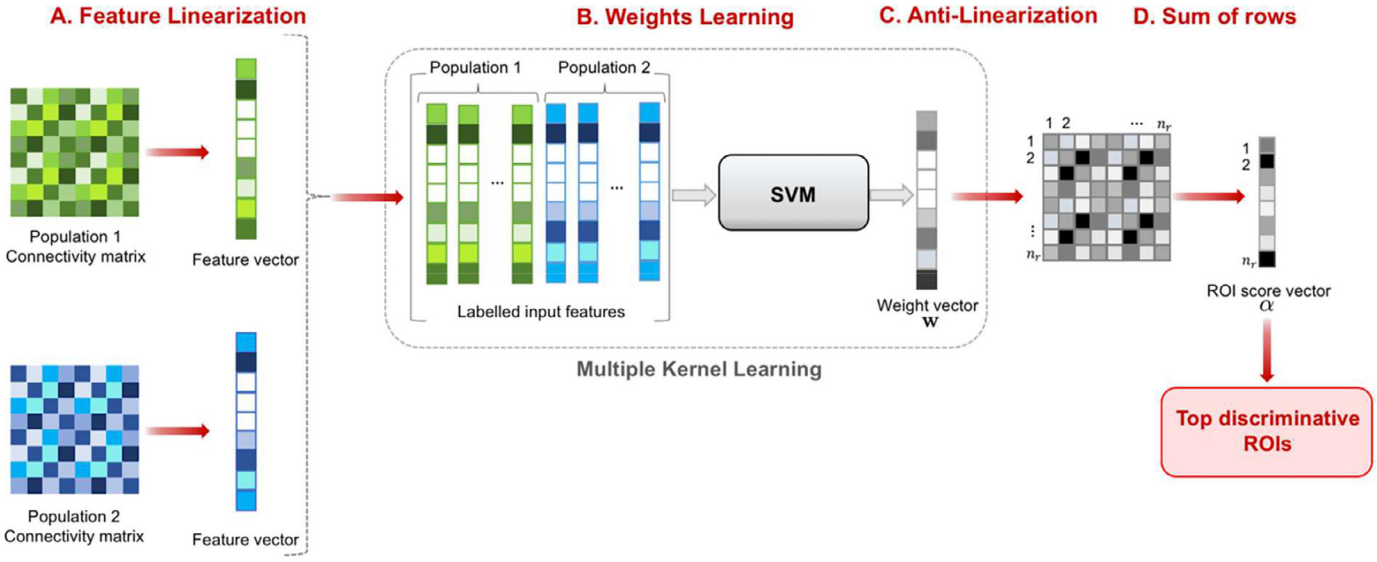

Fig. 6. Identification of the top discriminative ROIs using Multiple Kernel Learning (MKL). (A) We vectorized the upper triangular part of each population matrix to generate a feature vector for each connectional network. (B) Using multiple kernel learning (MKL), we obtain a weight vector $\boldsymbol{w}$ quantifying the discriminability of each brain feature (i.e., brain connectivity between two regions of interest (ROIs). (C) We use anti-linearization to transform the weight vector into a matrix where each element represents the weight of a connectivity between two ROIs. (D) By summing up the columns of the produced matrix we get a score vector denoting the discriminability of each ROI.

Finally, we select the top discriminative ROIs using the highest scores α_i, where $1 \leq i \leq n_r$ (Fig. 6).

4. Results

For comparative evaluation, we benchmarked netNorm against SCA method introduced in (Dhifallah and Rekik, 2019) in addition to four baseline methods, relying on either of the following two key steps or both: (1) we merge the different views at the individual level, and (2) we fuse the resulting views from step (1) at the population level into a single network representing the final CBT. Both steps are conducted using one of the following merging techniques: linear fusion (average of different views) or non-linear similarity network fusion (SNF) (Wang et al., 2014). These four include SNF-SNF (SS), Average-Average (AA), SNF-Average (SA), and Average-SNF (AS). The number of iterations used in SNF is set to $N_t = 20$ to guarantee its convergence as recommended in (Wang et al., 2014). We empirically set the number of nearest neighbors to $q = 20$.

CBT representativeness and centredness. In order to evaluate the representativeness of the proposed CBT, we computed the mean Frobenius distance between the estimated brain network and the different views in the population for baseline methods as well as the proposed framework for both hemispheres (LH: the left hemisphere and RH: the right hemisphere). Table 3 displays the mean Frobenius distance between the estimated CBTs calculated using the whole dataset for baseline methods as well as the proposed framework. We note that our proposed CBT remarkably and consistently outperforms conventional techniques by achieving the minimum distance for all datasets using both hemispheres offering the most centered brain template for each population. Fig. 7 further plots the mean normalized distances between the estimated CBT and all views in the population for each hemisphere in our four datasets (AD, LMCI, ASD, NC) using 5-fold cross validation

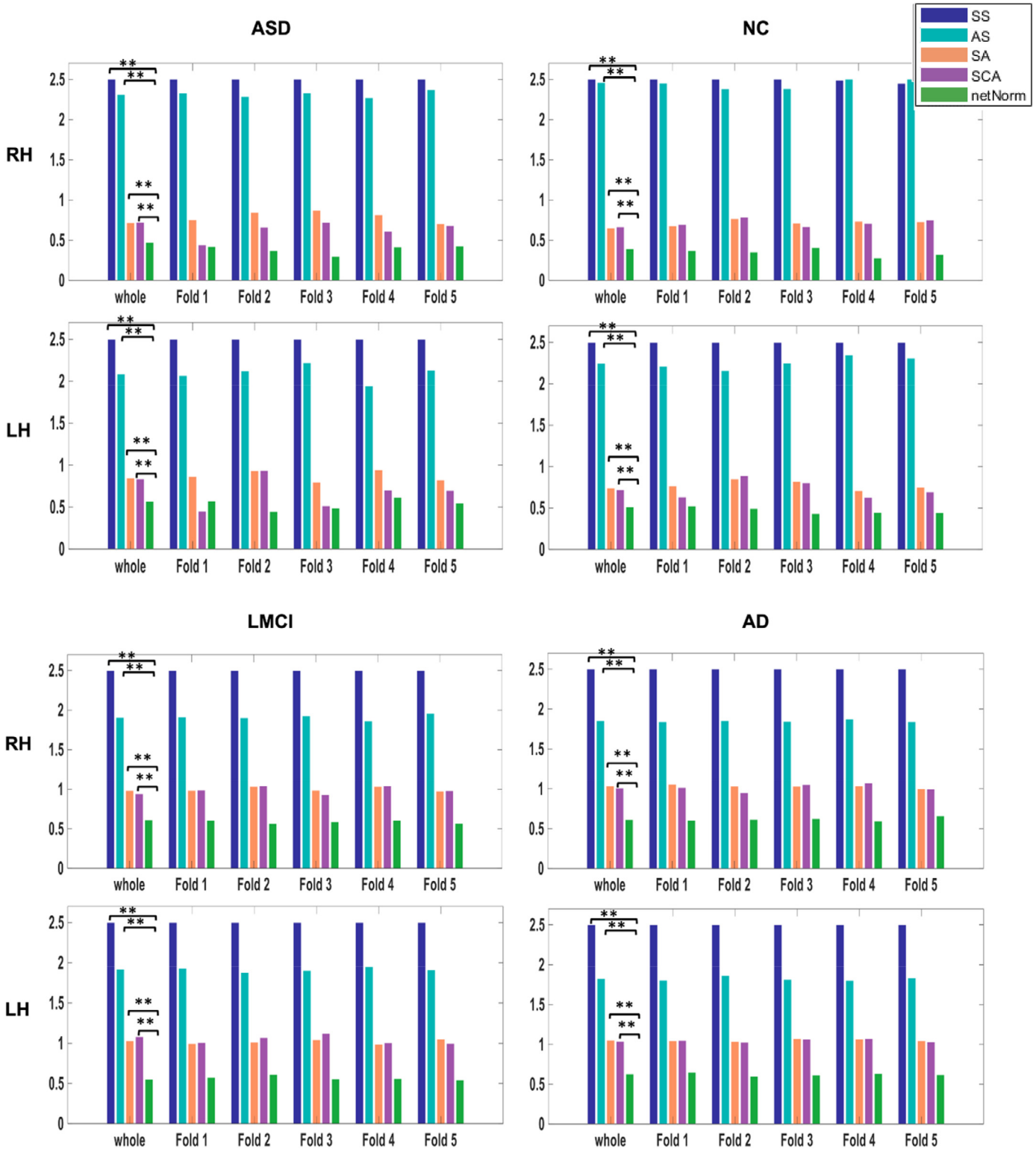

Fig. 7. Evaluation of netNorm performance. Average Frobenius distance between the estimated connectional brain template (CBT) and all views in the original space using netNorm and benchmark methods for the left and right cortical hemispheres in ASD, NC, LMCI and AD populations. In addition to SCA technique introduced in (Dhifallah and Rekik, 2019), comparison methods apply linear averaging (A) or nonlinear similarity network fusion (S) techniques in the following two steps: (i) merging brain network views for each subject into a single network, and (ii) merging brain networks across all subjects. (**) for p-value < 0.001 using two-tailed paired t-test.

Table 3
Normalized mean Frobenius distance between the estimated connectional brain template and the different connectional brain views using all subjects in different datasets. LMCI: late mild cognitive impairment. AD: Alzheimer's disease. NC: normal controls. ASD: autism spectrum disorder.

Datasets	ASD		NC		LMCI		AD	
	LH	RH	LH	RH	LH	RH	LH	RH
AA ($\times 10^{-2}$) (Tapez une équation ici.	11.54	11.01	13.95	13.41	7.71	5.39	6.25	5.48
SS	2.50	2.50	2.50	2.50	2.50	2.50	2.50	2.50
AS	2.08	2.31	2.25	2.46	1.92	1.90	1.82	1.85
SA	0.85	0.72	0.74	0.65	1.03	0.98	1.05	1.03
SCA (Dhifallah and Rekik, 2019)	0.84	0.73	0.73	0.65	1.06	0.92	1.02	1.01
netNorm	**0.57**	**0.47**	**0.51**	**0.39**	**0.55**	**0.61**	**0.62**	**0.61**

Table 4
Matching rate in% between top discriminative ROIs identified by MKL method and the difference between connectional templates estimated for ASD/NC and AD/LMCI populations.

Datasets	AD/LMCI		ASD/NC	
	LH	RH	LH	RH
AA	66.67	73.34	53.54	53.54
AS	46.67	46.67	40.00	46.67
SA	73.34	73.34	53.34	73.34
SS	75.27	72.54	16.92	16.65
SCA (Dhifallah and Rekik, 2019)	73.33	66.7	60	60
netNorm	**86.66**	**80.00**	**66.67**	**66.67**

to evaluate the generalizability of our results across folds and when scaling up the data (i.e., considering the whole dataset). We note that netNorm consistently outperforms comparison methods in terms of centredness when applied to all populations using both hemispheres for a p-value < 0.001 using two-tailed paired *t*-test. In fact, the estimated CBTs using netNorm constantly have the minimum normalized mean distance to all views across all subjects followed by SCA (Dhifallah and Rekik, 2019), SA, AS, SS and AA techniques, respectively. We did not include the results of AA method in Fig. 7 since its distance values largely exceed the average range of other distances.

CBT discriminability. In addition to being well-centered, we demonstrate that netNorm produces well-representative templates in terms of preserving the distinctive traits for a given population. Therefore, we conducted a comparative study between ASD and NC populations (respectively LMCI and AD populations) for both hemispheres using the estimated CBTs. More specifically, we identified the top 15 discriminative ROIs distinguishing between two groups (ASD vs. NC and AD vs. LMCI) for each hemisphere using the absolute difference between the CBTs estimated using netNorm and each of the baseline methods (AA, SA, AS, SS and SCA). Then, we calculated the overlap between the most discriminative anatomical ROIs revealed using our method and those identified using MKL. Table 4 displays the overlap in% between ranked most discriminative ROIs identified by (i) MKL and (ii) the absolute difference between the two estimated CBTs of the comparison methods, respectively. We note that netNorm, overall, achieved a significantly ($p < 0.05$) larger overlap in terms of top discriminative ROIs compared with those generated by comparison techniques across all datasets except for the right hemisphere in ASD/NC populations, where it fell behind SA technique. Specifically, netNorm reached an overlap percentage of 86% for distinguishing AD from LMCI subjects using the left hemisphere and 80% for the right hemisphere.

In Fig. 8, we visualize the top 15 discriminative ROIs selected using MKL and netNorm respectively. We represent each of the selected ROIs using its normalized score $\boldsymbol{\alpha}$ depicting its discriminability power in distinguishing between different populations for all datasets using both hemispheres. We note that, the most discriminative ROIs selected by netNorm in distinguishing between LMCI and AD populations include the pericalcarine cortex (region 21) (Wee et al., 2013) and the entorhinal cortex (region 6) associated with a decreased volume in subjects with Alzheimer's disease in comparison to those with mild cognitive impairment (Devanand et al., 2007) for the right hemisphere and the pericalcarine cortex (region 21) and the Rostral middle frontal gyrus (region 27) (Wee et al., 2013) for the left hemisphere, respectively.

Thus, by applying netNorm to healthy and disordered populations, we show that the estimated CBTs reliably spot altered brain regions differentiating healthy and pathological groups. More importantly, Table 5 displays the top 5 discriminative ROIs distinguishing between healthy and autistic subjects (ASD vs. NC populations) using netNorm for both RH and LH, which are consistent with previous findings on atypical regions in autistic subjects in the literature. More specifically, we note that both the pericalcarine cortex and the entorhinal cortex are selected as the most discriminative ROIs determined by netNorm that differentiate between healthy and autistic subjects for both hemispheres. These regions are known to be related to ASD (Zielinski et al., 2014; Wegiel et al., 2010). In particular, the entorhinal cortex is highly correlated with hyperactivity, aggression and self-injurious behavior in autistic subjects.

5. Discussion

In this paper, we introduced netNorm, a novel framework for connectional brain template estimation that leverages complementary information offered by different brain views for a population of multi-view brain networks. We first built multi-view brain connections between different regions of the brain for a population of subjects, then we defined a cross-view feature vector between each pair of ROIs for each individual in the population. In order to investigate the inter-relationship between different subjects in the population at a local scale, we constructed a high-order graph for each pairwise connection capturing the dissimilarities between the cross-view feature vectors across all subjects. A selection process is then applied to construct a multi-view population representative tensor through selecting the most common cross-view feature vectors among the population. The estimated CBT is then generated by fusing the different views of the estimated tensor. We aimed to use the produced connectional templates in order to identify potential biomarkers for neurodevelopmental (ASD) and neurodegenerative (AD) disorders.

CBT representativeness and centeredness. Our proposed method achieved the best performance in terms of centredness where the estimated CBT had the minimum mean distance to all network views in the population (Fig. 7, Table 3). These results can be explained by the fact that while conventional methods (AA, AS, SA, SS) integrate the network views *equally* by merging them at a global scale, whereas netNorm learns how to fuse them at a local

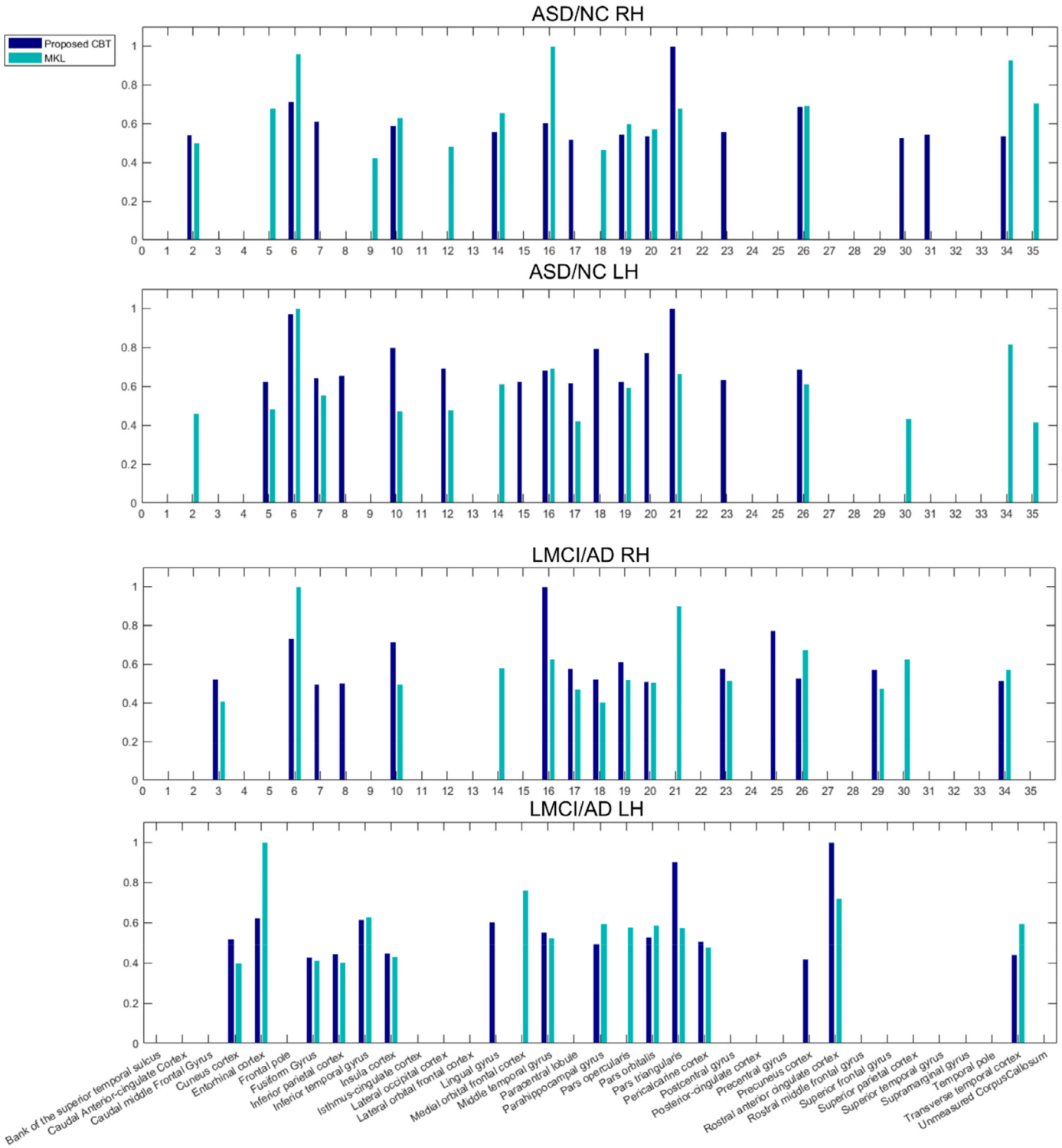

Fig. 8. Assessing the discriminability of the estimated population-specific connectional brain template by netNorm. We identify top 15 discriminative ROIs of LH using (i) multiple-kernel learning (MKL) and (ii) the template absolute difference between two brain populations for the right and left hemispheres (RH and LH).

scale by first selecting for each local pairwise connection between two ROIs the most representative cross-view feature vector in the population. More specifically, through building a high-order graph that captures the dissimilarities between different feature vectors across all subjects, netNorm builds a population representative tensor including feature vectors having the minimum distance in the graph. Therefore, instead of equally combining feature vectors across the whole population (e.g. through average or SNF), netNorm only selects the most common subject-specific feature vectors. The obtained tensor is a mosaic representation of the whole population that occupies a centered location to all subjects in the group. Thus, through satisfying the centredness criteria of the population representative tensor, netNorm ensures the centredness of the estimated CBT.

CBT discriminability. Different studies have shown that the complementary information offered by different brain modalities

Table 5
Top 5 discriminative regions of interest (ROIs) in the left and right hemispheres distinguishing between normal controls (NC) and autistic (ASD) subjects identified by computing the absolute difference between ASD and NC estimated CBTs built using netNorm.

	Top 5 discriminative ROIs	Behavioural effect in autism	ROI representation
Left Hemisphere	Pericalcarine cortex	Thicker cortex in autistic children in comparison to NC (Zielinski et al., 2014).	
	Entorhinal cortex	Hyperactivity, aggression and self-injurious behaviour (Wegiel et al., 2010).	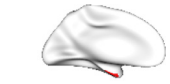
	Isthmus cingulate cortex	Impairment in social behavior (Doyle-Thomas et al., 2013).	
	Pars opercularis	Social communication problems (Yamasaki et al., 2010).	
	Pars triangularis	Language impairment (De Fossé et al., 2004)	
Right Hemisphere	Pericalcarine cortex	Thicker cortex in autistic children in comparison to NC (Zielinski et al., 2014).	
	Entorhinal cortex	Hyperactivity, aggression and self-injurious behavior (Wegiel et al., 2010).	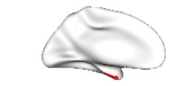
	Rostral anterior cingulate cortex	Aggression (Wegiel et al., 2010).	
	Fusiform Gyrus	Difficulties in face perception and persons' recognition (Van Kooten et al., 2008; Waiter et al., 2004).	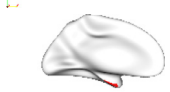
	Parahippocampal gyrus	Abnormal social cognition function (Xiaoyan et al., 2008).	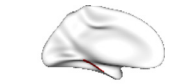

play an important role in identifying potential biomarkers for neurological disorders (Apostolova et al., 2010; de Leon et al., 2007). Defining a unified representation of a population of multi-view brain networks represents a key step for comparative studies. A naive practice in defining a population's template is by averaging the population's different views. However, this may not be enough to effectively merge complementary information and preserve the population's discriminative traits. In this paper, one important advantage of our proposed technique is its discriminative power in distinguishing between different populations as shown in Table 4 and Fig. 8. These results indicate the effectiveness of the proposed framework against *inter-subject variability* while enforcing the population's common and distinct traits. This can be explained, first, by the fact that the estimated CBT occupies the minimum distance compared to all subjects in the population which results in minimizing the inter-individual variability. Second, through defining a selection process that only takes into account the most common cross-view feature vectors across the whole population, netNorm builds a selective and reliable multi-view representation of the population before applying the final fusion process. Therefore, through constructing a high-order graph that captures the commonality aspect of each feature vector across subjects, netNorm explores the global architecture between subjects at the feature vector scale by exploring their inter-connections. In addition, through applying SNF for non-linear fusion of the representative views, netNorm explores the complementary information offered by different representative brain modalities. SNF fuses complementary data lying on different manifolds by an iterative process that adds strong connections between different networks to one another while discarding weak connections (Wang et al., 2014). Therefore, ensuring a more robust representation of a population's connectional characteristics and conserving its distinct traits. We believe that our proposed method will pave the way for more representative CBT estimation techniques, stimulating a deeper understanding of neurodegenerative and neurodevelopmental diseases using different data sources.

We display in Table 5 the top 5 discriminative ROIs distinguishing between healthy and autistic subjects for the right and left hemispheres by computing the absolute difference between the estimated CBTs and pinning down regions with highest differences. We show that the pericalcarine cortex followed by the entorhinal cortex represent the most 2 discriminative ROIs for

both hemispheres. We note that the human brain presents hemispheric asymmetries that occur by nature (Wada et al., 1975) or through the asymmetric influence of autism (Chiron et al., 1995; Herbert et al., 2004), which explains the asymmetry between the remaining discriminative regions for both hemispheres. We also note that our findings are consistent with previous studies where most of the identified ROIs obtained using netNorm are correlated with behavioral impairments in autistic subjects. Particularly, for the left hemisphere the isthmus cingulate cortex which is responsible for social behavior impairment (Doyle-Thomas et al., 2013), the pars opercularis affecting the social communication skills and the pars triangularis responsible for language impairment were identified as discriminative ROIs between ASD and NC groups. For the right hemisphere, however, we identified other discriminative regions including the rostral anterior cingulate cortex explaining the aggressive behavior in autistic subjects (Wegiel et al., 2010), the fusiform gyrus responsible for the difficulties in face perception and persons' recognition (Van Kooten et al., 2008; Waiter et al., 2004) and the parahippocampal gyrus affecting the social cognitive function for ASD subjects (Xiaoyan et al., 2008).

Limitations. Our work has a few limitations. First, we evaluated netNorm on morphological connectomic data using Desikan-Killiany brain atlas, yet our framework is a generic method that can be applied to different connectional modalities (e.g., functional and structural connectomes) and using different brain parcellation (Glasser et al., 2016). We note that, for a given population, the same parcellation template shall be consistently used across all network modalities and across all subjects. Second, we only tested netNorm on morphological brain networks capturing different attributes. For future work, we can consider combining different brain views derived from different imaging modalities (e.g., structural and morphological brain networks) in order to explore diverse and complementary information. Third, we used Euclidean distance as a dissimilarity metric to build a high-order graph between different cross-view feature vectors, which alternatively can be *learned* to better model the high dimensionality of feature vectors derived from multi-view networks. Forth, although we identified morphological ROIs biomarkers for ASD and AD diseases, we did not examine the connectional aspect between these regions. These unexplored directions can be further investigated in our future work.

6. Conclusion

In this paper, we unprecedentedly propose netNorm framework for normalizing a population of multi-view brain networks by estimating a well-representative and centered connectional brain template using a selective fusion process. Specifically, we applied a selection strategy for building a multi-view population representative tensor based on a commonality criterion for cross-view feature vectors' selection among all subjects. Then we constructed the final template by non-linearly fusing the different representative views. The proposed method outperformed the baseline methods on four datasets composed of ASD, NC, AD, and LMCI subjects, respectively, in terms of (i) centredness and representativeness compared to all subjects and all views in the population and (ii) discriminability in preserving the population characteristics. In our future work, we will explore manifold learning techniques to enhance the non-linear fusion process. Also, we will evaluate our framework on other types of brain network views including positive and negative values (e.g. functional brain connectivity) on larger datasets.

Declaration of competing interest

The authors declare no conflict of interest.

Acknowledgments

Data collection and sharing for this project was funded by the Alzheimer's Disease Neuroimaging Initiative (ADNI) (National Institutes of Health Grant U01 AG024904) and DOD ADNI (Department of Defense award number W81XWH-12–2–0012). ADNI is funded by the National Institute on Aging, the National Institute of Biomedical Imaging and Bioengineering, and through generous contributions from the following: AbbVie, Alzheimer's Association; Alzheimer's Drug Discovery Foundation; Araclon Biotech; BioClinica, Inc.; Biogen; Bristol-Myers Squibb Company; CereSpir, Inc.; Cogstate; Eisai Inc.; Elan Pharmaceuticals, Inc.; Eli Lilly and Company; EuroImmun; F. Hoffmann-La Roche Ltd and its affiliated company Genentech, Inc.; Fujirebio; GE Healthcare; IXICO Ltd.; Janssen Alzheimer Immunotherapy Research & Development, LLC.; Johnson & Johnson Pharmaceutical Research & Development LLC.; Lumosity; Lundbeck; Merck & Co., Inc.; Meso Scale Diagnostics, LLC.; NeuroRx Research; Neurotrack Technologies; Novartis Pharmaceuticals Corporation; Pfizer Inc.; Piramal Imaging; Servier; Takeda Pharmaceutical Company; and Transition Therapeutics. The Canadian Institutes of Health Research is providing funds to support ADNI clinical sites in Canada. Private sector contributions are facilitated by the Foundation for the National Institutes of Health (www.fnih.org). The grantee organization is the Northern California Institute for Research and Education, and the study is coordinated by the Alzheimer's Therapeutic Research Institute at the University of Southern California. ADNI data are disseminated by the Laboratory for Neuro-Imaging at the University of Southern California.

References

Apostolova, L.G., Hwang, K.S., Andrawis, J.P., Green, A.E., Babakchanian, S., Morra, J.H., Cummings, J.L., Toga, A.W., Trojanowski, J.Q., Shaw, L.M., Jack Jr., C.R., Petersen, R.C., Aisen, P.S., Jagust, W.J., Koeppe, R.A., Mathis, C.A., Weiner, M.W., Thompson, P.M., 2010. 3D PIB and CSF biomarker associations with hippocampal atrophy in ADNI subjects. Neurobiol. Aging 31, 1284–1303.

Chiron, C., Leboyer, M., Leon, F., Jambaque, L., Nuttin, C., Syrota, A., 1995. Spect of the brain in childhood autism: evidence for a lack of normal hemispheric asymmetry. Dev. Med. Child Neurol. 37, 849–860.

De Fossé, L., Hodge, S.M., Makris, N., Kennedy, D.N., Caviness, V.S., McGrath, L., Steele, S., Ziegler, D.A., Herbert, M.R., Frazier, J.A., Tager-Flusberg, H., Harris, G.J., 2004. Language-association cortex asymmetry in autism and specific language impairment. Ann. Neurol. 56, 757–766.

Desikan, R.S., Ségonne, F., Fischl, B., Quinn, B.T., Dickerson, B.C., Blacker, D., Buckner, R.L., Dale, A.M., Maguire, R.P., Hyman, B.T., Albert, M.S., Killiany, R.J., 2006. An automated labeling system for subdividing the human cerebral cortex on mri scans into gyral based regions of interest. NeuroImage 104, 968–980.

Devanand, D.P., Pradhaban, G., Liu, X., Khandji, A., De Santi, S., Segal, S., Rusinek, H., Pelton, G.H., Honig, L.S., Mayeux, R., Stern, Y., Tabert, M.H., de Leon, M.J., 2007. Hippocampal and entorhinal atrophy in mild cognitive impairment prediction of Alzheimer disease. Neurology 11, 828–836.

Dhifallah, S., Rekik, I., 2019. Clustering-based multi-view network fusion for estimating brain network atlases of healthy and disordered populations. J. Neurosci. Method. 311, 426–435.

Dickie, D.A., Shenkin, S.D., Anblagan, D., Lee, J., Cabez, M.B., Rodriguez, D., Boardman, J.P., Waldman, A., Job, D.E., Wardlaw, J.M., 2017. Whole brain magnetic resonance image atlases: a systematic review of existing atlases and caveats for use in population imaging. Front. Neuroinformat. 11, 1.

Doyle-Thomas, K.A.R., Kushki, A., Duerden, E.G., Taylor, M.J., Lerch, J.P., Soorya, L.V., Wang, A.T., Fan, J., Anagnostou, E., 2013. The effect of diagnosis, age, and symptom severity on cortical surface area in the cingulate cortex and insula in autism spectrum disorders. J. Child Neurol. 28, 732–739.

Essen, D.C.V., Glasser, M.F., 2016. The human connectome project: progress and prospects. Cerebrum: The Dana forum on brain science (Dana Foundation, 2016).

Essen, V., 1997. A tension-based theory of morphogenesis and compact wiring in the central nervous system. Nature 385, 313.

Farrell, C., Chappell, F., Armitage, P.A., Keston, P., MacLullich, A., Shenkin, S., Wardlaw, J.M., 2009. Development and initial testing of normal reference MR images for the brain at ages 65–70 and 75–80 years. Eur. Radiol. 19, 177–183.

Fischl, B., 2012. FreeSurfer. Neuroimage 62, 774–781.

Fischl, B., Van der Kouwe, A., Destrieux, C., Halgren, E., Ségonne, F., Salat, D.H., Busa, E., Seidman, L.J., Goldstein, J., Kennedy, D., Caviness, V., Makris, N., Rosen, B., Dale, A.M., 2004. Automatically parcellating the human cerebral cortex. Cerebral Cortex 14, 11–22.

Glasser, M.F., Coalson, T.S., Robinson, E.C., Hacker, C.D., Harwell, J., Yacoub, E., Ugurbil, K., Andersson, J., Beckmann, C.F., Jenkinson, M., Smith, S.M., Van Essen, D.C., 2016. A multi-modal parcellation of human cerebral cortex. Nature 536, 171–178.

Hardan, A.Y., Libove, R.A., Keshavan, M.S., Melhem, N.M., Menshew, N.J., 2009. A preliminary longitudinal magnetic resonance imaging study of brain volume and cortical thickness in autism. Biol. Psychiatry 66, 320–326.

Herbert, M.R., Ziegler, D.A., Deutsch, C., O'Brien, L.M., Kennedy, D.N., Filipek, P., Bakardjiev, A., Hodgson, J., Takeoka, M., Makris, N., et al., 2004. Brain asymmetries in autism and developmental language disorder: a nested whole-brain analysis. Brain 128, 213–226.

Hinrichs, C., Singh, V., Xu, G., Johnson, S.C., 2011. Predictive markers for ad in a multi-modality framework: an analysis of mci progression in the ADNI population. Neuroimage 55, 574–589.

Holmes, A.J., Hollinshead, M.O., O'Keefe, T.M., Petrov, V.I., Fariello, G.R., Wald, L.L., Fischl, B., Rosen, B.R., Mair, R.W., Roffman, J.L., Smoller, J.W., Buckner, R.L., 2015. Brain genomics superstruct project initial data release with structural, functional, and behavioral measures. Sci. Data 2, 15–31.

Jbabdi, S., Sotiropoulos, S.N., Haber, S.N., Van Essen, D.C., Behrens, T.E., 2015. Measuring macroscopic brain connections in vivo. Nature Neurosci. 18, 1546.

de Leon, M.J., Mosconi, L., Li, J., De Santi, S., Yao, Y., Tsui, W.H., Pirraglia, E., Rich, K., Javier, E., Brys, M., Glodzik, L., Switalski, R., Saint Louis, L.A., Pratico, D., 2007. Longitudinal CSF isoprostane and MRI atrophy in the progression to AD. J. Neurol. 254, 1666–1675.

Lerch, J.P., Van der Kouwe, A.J.W., Raznahan, A., Paus, T., Johansen-Berg, H., Miller, K.L., Smith, S.M., Fischl, B., Sotiropoulos, S.N., 2017. Studying neuroanatomy using MRI. Nature Neurosci. 20, 314.

Lisowska, A., Rekik, I.Alzheimer's Disease Neuroimaging Initiative, 2018. Joint pairing and structured mapping of convolutional brain morphological multiplexes for early dementia diagnosis. Brain Connect. 9 (1), 22–36.

Mahjoub, I., Mahjoub, M.A., Rekik, I., 2018. Brain multiplexes reveal morphological connectional biomarkers fingerprinting late brain dementia states. Sci. Rep. 8, 4103.

Martino, A.D., Yan, C.G., Li, Q., Denio, E., Castellanos, F.X., Alaerts, K., Anderson, J.S., Assaf, M., Bookheimer, S.Y., Dapretto, M., Deen, B., Delmonte, S., Dinstein, I., Ertl-Wagner, B., Fair, D.A., Gallagher, L., Kennedy, D.P., Keown, C.L., Keysers, C., Lainhart, J.E., Lord, C., Luna, B., Menon, V., Minshew, N.J., Monk, C.S., Mueller, S., Müller, R.A., Nebel, M.B., Nigg, J.T., O'Hearn, K., Pelphrey, K.A., Peltier, S.J., Rudie, J.D., Sunaert, S., Thioux, M., Tyszka, J.M., Uddin, L.Q., Verhoeven, J.S., Wenderoth, N., Wiggins, J.L., Mostofsky, S.H., Milham, M.P., 2014. The autism brain imaging data exchange: towards a large-scale evaluation of the intrinsic brain architecture in autism. Mol. Psychiatry 19, 659.

McEvoy, L.K., Fennema-Notestine, C., Cooper Roddey, J., Hagler, D.J., Holland, D., Karow, D.S., Pung, C.J., Brewer, J.B., Dale, A.M., 2009. Alzheimer disease: quantitative structural neuroimaging for detection and prediction of clinical and structural changes in mild cognitive impairment. Radiology 251, 195–205.

Mueller, S.G., Weiner, M.W., Thal, L.J., Petersen, R.C., Jack, C., Jagust, W., Trojanowski, J.Q., Toga, A.W., Beckett, L., 2005. The alzheimer's disease neuroimaging initiative. Neuroimag. Clin. 15, 869–877.

Park, H.J., Friston, K., 2013. Structural and functional brain networks: from connections to cognition. Science 342, 1238411 (2013).

Raeper, R., Lisowska, A., Rekik, I., 2018. Cooperative correlational and discriminative ensemble classifier learning for early dementia diagnosis using morphological brain multiplexes. IEEE Access 6, 43830–43839.

Rekik, I., Li, G., Lin, W., Shen, D., 2017. Estimation of brain network atlases using diffusive-shrinking graphs: application to developing brains. In: International Conference on Information Processing in Medical Imaging, pp. 385–397.

Ridgway, G.R., Lehmann, M., Barnes, J., Rohrer, J.D., Warren, J.D., Crutch, S.J., Fox, N.C., 2012. Early-onset alzheimer disease clinical variants: multivariate analyses of cortical thickness. Neurology 79, 80–84.

Rickert, J., 1986. The Fromm-Marcuse debate revisited. Theory Soc. 15, 351–400.

Seidlitz, J., Váša, F., Shinn, M., Garcia, R.R., Whitaker, K.J., Vértes, P.E., Wagstyl, K., Reardon, P.K., Clasen, L., Liu, S., Messinger, A., Leopold, D.A., Fonagy, P., Dolan, R.J., Jones, P.B., Goodyer, I.M., Raznahan, A., Bullmore, E.T., 2018. Morphometric similarity networks detect microscale cortical organization and predict inter-individual cognitive variation. Neuron 97, 231–247.

Soussia, M., Rekik, I., 2018. Unsupervised manifold learning using high-order morphological brain networks derived from T1-w MRI for autism diagnosis. Front. Neuroinformat. 12, 70.

Thung, K.H., Wee, C.Y., Yap, P.T., Shen, D., 2014. Neurodegenerative disease diagnosis using incomplete multi-modality data via matrix shrinkage and completion. Neuroimage 91, 386–400.

Tong, T., Gray, K., Gao, Q., Chen, L., Rueckert, D., 2015. "Nonlinear graph fusion for multi-modal classification of Alzheimer's disease". In: International Workshop on Machine Learning in Medical Imaging. Springer, pp. 77–84.

Van Kooten, I.A.J., Palmen, S.J.M.C., Von Cappeln, P., Steinbusch, H.W.M., Korr, H., Heinsen, H., Hof, P.R., Van Engeland, H., Schmitz, C., 2008. Neurons in the fusiform gyrus are fewer and smaller in autism. Brain 131, 987–999.

Wada, J.A., Clarke, R., Hamm, A., 1975. Cerebral hemispheric asymmetry in humans: cortical speech zones in 100 adults and 100 infant brains. Arch. Neurol. 32, 239–246.

Wallace, G.L., Dankner, N., Kenworthy, L., Giedd, J.N., Martin, A., 2010. Age-related temporal and parietal cortical thinning in autism spectrum disorders. Brain 133, 3745–3754.

Waiter, G.D., Williams, J.H.G., Murray, A.D., Gilchrist, A., Perrett, D.I., Whiten, A., 2004. A voxel-based investigation of brain structure in male adolescents with autistic spectrum disorder. NeuroImage 22, 619–625.

Wang, B., Mezlini, A.M., Demir, F., Fiume, M., Tu, Z., Brudno, M., Haibe-Kains, B., Goldenberg, A., 2014. Similarity network fusion for aggregating data types on a genomic scale. Nature Method. 11, 333.

Wee, C.Y., Yap, P.T., Shen, D., 2013. Prediction of Alzheimer's disease and mild cognitive impairment using cortical morphological patterns. Human Brain Mapp. 12, 3411–3425.

Wegiel, J., Kuchna, I., Nowicki, K., Imaki, H., Wegiel, J., Marchi, E., Ma, S.Y., Chauhan, A., Chauhan, V., Bobrowicz, T.W., de Leon, M., Saint Louis, L.A., Cohen, I.L., London, E., Brown, W.T., Wisniewski, T., 2010. The neuropathology of autism: defects of neurogenesis and neuronal migration, and dysplastic changes. Acta Neuropathol. 119, 755–770.

Wu, G., Kim, M., Sanroma, G., Wang, Q., Munsell, B.C., Shen, D., 2015. Hierarchical multi-atlas label fusion with multi-scale feature representation and label-specific patch partition. NeuroImage 104, 34–46.

Wu, G., Jia, H., Wang, Q., Shen, D., 2011. SharpMean: groupwise registration guided by sharp mean image and tree-based registration. NeuroImage 56, 1968–1981.

Xiaoyan, K., Shanshan, H., Tianyu, T., Bing, Z., Huiguo, L., Yueyue, H., Zhenyu, Z., Zongcai, R., Zuhong, L., Guotai, T., Yijun, L., 2008. Voxel-based morphometry study on brain structure in children with high-functioning autism. Neuroreport 19, 921–925.

Yamasaki, S., Yamasue, H., Abe, O., Suga, M., Yamada, H., Inoue, H., Kuwabara, H., Kawakubo, Y., Yahata, N., Aoki, S., Kano, Y., Kato, N., Kasai, K., 2010. Reduced gray matter volume of pars opercularis is associated with impaired social communication in high-functioning autism spectrum disorders. Biol. Psychiatry 68, 1141–1147.

Yuan, L., Wang, Y., Thompson, P.M., Narayan, V.A., Ye, J., 2012. Multi-source feature learning for joint analysis of incomplete multiple heterogeneous neuroimaging data. Neuroimage 61, 622–632.

Zhang, D., Wang, Y., Zhou, L., Yuan, H., Shen, D., 2011. Multimodal classification of Alzheimer's disease and mild cognitive impairment. Neuroimage 55, 856–867.

Zielinski, B.A., Prigge, M.B.D., Nielsen, J.A., Froehlich, A.L., Abildskov, T.J., Anderson, J.S., Fletcher, P.T., Zygmunt, K.M., Travers, B.G., Lange, N., Alexander, A.L., Bigler, E.D., Lainhart, J.E., 2014. Longitudinal changes in cortical thickness in autism and typical development. Brain 137, 1799–1812.